Combining molecular motion with a 2,6-diiodo BODIPY to engineer highly anisotropic thermomechanical properties in organic binary and ternary molecular materials

Babak Tahmouresilerd,†a Jinchun Qiu,†a Gary C. George III,†a,b Vivian Woh,a Miranda C. Andrews,a Shiva Moaven,a Daniel K. Unruh,a Kristin M. Hutchins,a,b* and Anthony F. Cozzolinoa,*

^aDepartment of Chemistry and Biochemistry, Texas Tech University, Box 1061, Lubbock, Texas 79409-1061, United States

^bDepartment of Chemistry, University of Missouri, 601 S College Ave, Columbia, Missouri 65211, United States

ABSTRACT: Designing materials to have three unique, but predictable thermal expansion axes, represents a major challenge. Inorganic materials and hybrid frameworks tend to crystalize in high symmetry space groups, which necessarily limits this by affording isotropic behavior. On the other hand, molecular organic materials tend to crystallize in lower symmetry space groups, offering significant opportunity to achieve anisotropic properties. The challenge arises in self-assembling the organic components into a predictable arrangement to afford predictable thermal expansion properties. Here, we demonstrate a design strategy for engineering organic solid-state materials that exhibit anisotropic thermomechanical behaviors. Presented are a series of multicomponent solids wherein one component features a BODPIY core strategically decorated with orthogonal hydrogen- and halogen-bond donor groups. A series of size-matched halogen-bond acceptors are used as the second component in each solid. By matching the molecular dimensions with the interaction strength, good control over the anisotropic thermal expansion of the molecular materials was obtained. Moreover, using shape-size mimicry and propensity for molecular motion, a rare ternary molecular system that is isostructural to the two binary solids was successfully achieved. The diiodo-functionalized BODIPY core in this study has been previously used in photocatalysts, and halogen bonding was hypothesized as a driving force; here, we provide corroborating solution and solid-state evidence of intermolecular halogen bonding in multi-component solids featuring a 2,6-diiodo BODIPY.

1. INTRODUCTION

The thermomechanical response of a molecular crystalline solid can be difficult to predict and control. Generally, thermal expansion with a coefficient (α_L) of less than 20 x $10^{-6}~K^{-1}$ is observed upon heating.^{1,2} This results from increased vibrational motions in all directions. Strategies for controlling the thermal response and achieving nonstandard thermal responses have slowly started to emerge³⁻ 6. While the desired thermal response depends on the real or perceived application, they generally can be categorized as isotropic or anisotropic, negative, zero, or positive.^{7,8} Materials that undergo negative thermal expansion have found use in optics, composites, and thermal expansion compensators, 9,10 while those that undergo positive thermal expansion are often used in sensors and actuators.^{4,11} The atomic/molecular displacements from the equilibrium position are anisotropic for bond stretching vibrational motions as well as for phonons that change intermolecular separations (Figure 1). Typically, for the same energy, a bond can be stretched further than it can be compressed. This results in thermal expansion. Large thermal expansion, therefore, correlates with shallow and highly anisotropic energy potentials between atoms/molecules in the solid state. In principle, thermal expansion along a given direction in molecular solids can be maximized by organizing molecules along their short axis by weak interactions. 12,13 Conversely, thermal expansion is minimized when long molecules are organized by strong intermolecular interactions along their long axis. In crystalline molecular solids, molecular thermal expansion contributes very little to the observed thermomechanical properties since the potentials associated with intramolecular vibrations are much higher than the potentials associated with longitudinal phonons (Figure 1). Following these arguments, it is the number and strength of intermolecular interactions over a given distance that should govern most of the observed thermomechanical behavior of crystalline molecular solids. Thus, gaining control over the intermolecular interaction identity and strength in three directions will enable control over the corresponding thermal expansion along those directions.

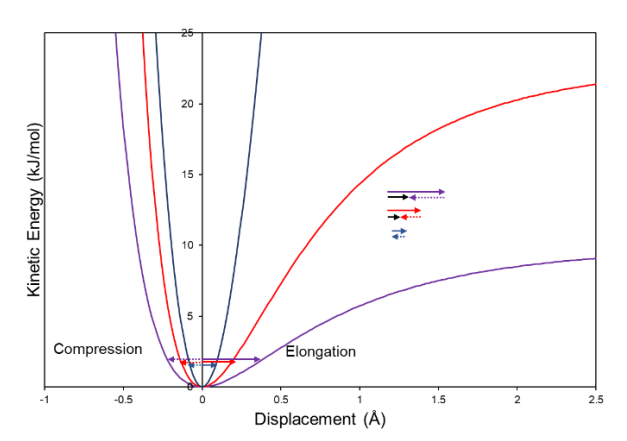


Figure 1. Kinetic energy surfaces representing displacement along O–H bond (blue, 458 kJ/mol modelled with Morse potential), 0···H hydrogen bond (red, 23 kJ/mol modelled with Lennard-Jones potential), and π ··· π stacking (purple, 10 kJ/mol modelled with Lennard-Jones potential). Arrows indicate elongation (solid) or compression (dotted) at a given kinetic energy. Resulting thermal expansion (elongation – compression) is depicted with black arrow.

Engineering highly anisotropic thermomechanical properties in molecular materials requires careful design strategies. One such strategy is to create a scissor-gate motif in one plane of the crystal. 14,15 Here, as one principal axis elongates, the other contracts. In this case, the changes in bond angles are primarily responsible for the observed behavior. An alternative strategy is to create space for lowenergy transverse phonons that will allow the system to contract along the longitudinal axis as the transverse modes become populated. 16,17

In the current study, the possibility of designing molecular crystals to have predictable thermal expansion along each principal axis is explored. The design principle proposed here is to organize molecules along their long axis through strong intermolecular interactions. Medium strength interactions will be used to control assembly (and thermal expansion) along the medium length molecular axis, and the weakest interactions will align with the shortest molecular axis. This strategy is illustrated in Figure 2. To achieve this, we propose to use a combination of three different interaction types: 1) strong halogen bonds (HaB), 2) weak/medium hydrogen bonds (HB) and 3) weak π - π interactions. Ideally, each of these interaction types should be orthogonal to each other and aligned with the molecular axis. Typically, multi-substituted, planar aromatic molecules that engage in π - π stacking interactions have functional groups substituted at angles other than 90° from each other. e.g., 120° for meta substitution or 180° for para substitution. Thus, equally important is the choice of scaffold on which to introduce these features. Motifs for (co-)crystal engineering using HaB typically rely on di- or multitopic perhalogenated iodoalkyl and iodoaryl systems,18-20 or iodoethynyl systems.^{21,22} Iodine was chosen to act as the halogen bond donor as it has been shown to facilitate the strongest halogens. 19,23 halogen bonds amongst the Perfluorination/perchlorination is generally required to introduce a sufficiently large maximum in the electrostatic

potential (V_{max}) at the iodine so as to predictably direct the formation of HaBs. To achieve the orthogonal distribution of the intermolecular interactions, the BODIPY molecule was chosen as a platform. The BODIPY fragment has been identified as being significantly electron withdrawing, comparable to a tosyl or a pentafluorophenyl group.²⁴ Recently, it was proposed that the formation of HaBs to an iodo-functionalized BODIPY molecule, influenced the intersystem crossing in solution.²⁵ In a separate study, a halogen bonding network was observed in the solid state between an iodo-functionalized BODIPY and a HaB acceptor on a neighboring BODIPY. It was determined that the presence of the HaBs had a marked influence on the photophysical properties in the solid state.²⁶ Iodine functionalized BODIPY systems have seen applications in photocatalysis, taking advantage of the high molar absorptivity of the BODIPY core and the heavy atom effect to facilitate intersystem crossing.27-32

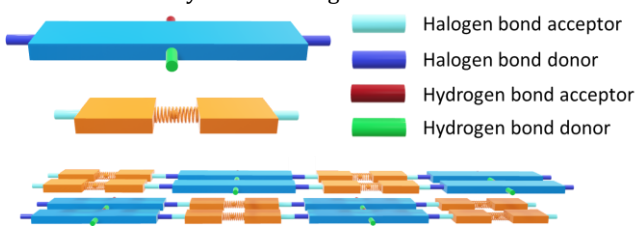


Figure 2. Idealized design strategy for highly anisotropic thermomechanical properties involving planar molecules with a combination of HaB and HB donors/acceptors.

In I₂BODIPY (Figure 3, 1), the near collinearity of the two C-I bonds when BODIPY is iodinated at the 2 and 6 positions makes it an ideal candidate for directing supramolecular self-assembly. A phenyl group at the 4-position would introduce a weak HB donor that could pair with the fluorine atoms which are moderately strong HB acceptors. Iodine can act as a HaB donor and acceptor, resulting in zig-zag chains that could undermine the proposed design strategy. Furthermore, polymorphism has been observed in 1, where either the iodine³³ or the fluorine³⁴⁻³⁶ atoms act as the HaB acceptors. To circumvent these issues, a cocrystallization³⁷ strategy (Figure 2) with bipyridyl HaB acceptors was adopted to achieve the desired orthogonal self-assembled solid-state materials. The cocrystallization strategy is based on the principles of Etter,38 wherein the strongest donor (iodine) will pair with the strongest acceptor (pyridine) to form the supramolecular synthon.39

I₂BODIPY (1)

Figure 3. Molecular structure of I₂BODIPY

This study demonstrates a hierarchical approach to achieving highly anisotropic thermal expansion that takes advantage of three different classes and strengths of supramolecular interactions arranged orthogonally around a molecule. The role that molecular motion can play in

modifying thermal expansion properties is also discussed. Furthermore, a rare example of a ternary cocrystal that is isostructural with the binary cocrystal systems was successfully designed and obtained using differences in propensity for molecular motion. Overall, we show the degree of thermal expansion along each direction is directly tied to the type and strength of supramolecular interaction sustaining the direction, showing the power of hierarchical and orthogonal self-assembly to achieve desired solid-state properties.

2. RESULTS AND DISCUSSION

Halogen bond donor ability of I2BODIPY

In order to confirm the HaB donor ability of **1**, an analysis of the wavefunction produced from DFT calculations (B97-D3, TZVP, ZORA) was performed. An electrostatic potential energy surface was generated (Figure 4), and it was noted that the maxima in the electrostatic potential (V_{max} , plotted on the 0.001 isosurface) exist along the extension of the CH bonds in the phenyl ring (91 kJ/mol) and along the extension of each C–I bond (86 kJ/mol). Despite the similarity in values, the high polarizability of the iodine will allow for a strong contribution from stabilizing dispersion forces that will supplement any electrostatically governed interaction at the iodine. The largest, in magnitude, minima on the electrostatic potential surface are localized on the F atoms (–125 kJ/mol) reflecting the distribution of the formal negative charge assigned to the boron atom.

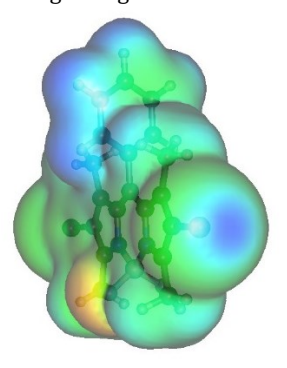


Figure 4. Electrostatic potential of $\bf 1$ mapped onto the 0.001 electron density isosurface. Color scale ranges from -160 (red) to 105 (blue) kJ/mol.

Preparation of I2BODIPY cocrystals

Compound **1** was prepared by following literature procedures. 29,40 Cocrystals of **1** with ditopic HaB acceptors BIPY (4,4'-bipyridine), BPA (1,2-bi(4-pyridyl)acetylene), Azo (4,4'-azopyridine), BPE (1,2-bi(4-pyridyl)ethylene) and Cl-Azo (3-chloro-4-[4-pyridinylazo]pyridine) were prepared by dissolving equimolar amounts (0.025 mmol) of **1** and HaB acceptors in 4 mL toluene and ethanol (1:1 ν/ν). Vials were monitored under slow-evaporation conditions and single crystals suitable for X-ray diffraction were observed after $\sim\!2$ days. Analysis of the unit cells was performed to identify new phases. The resulting structures are depicted with the observed I···N HaB motifs in Figure 5. 41 In order to study the thermal expansion behaviors, crystallographic data sets were collected on the same crystal

at 190 K, 210 K, 230 K, 250 K, 270 K, and 290 K with a heating/cooling rate of 2 K/min between temperatures.

Figure 5. Chemical structures of cocrystals in this work: (a) discrete assembly with ${\bf 1}$ and BIPY and (b) infinite assembly with ${\bf 1}$ and bridged bipyridines.

Discrete assembly of 1 and BIPY with binding energies

The ditopic HaB acceptor 4,4'-bipyridine (BIPY) was cocrystallized with 1 and the HaB motif is depicted in Figure 6. While it was anticipated that infinite chains would form through I···N HaBs, only discrete supramolecular trimers of 1 and BIPY with a formula 1_2 ·BIPY were observed. Even in the case where a three-fold excess of BIPY was present, the only cocrystals that grew had a unit cell that matched the 1_2 ·BIPY cocrystal. In the 1_2 ·BIPY cocrystal, both nitrogen atoms on BIPY are engaged in I···N HaBs with a distance of 2.997(3) Å at 190 K. The structure of 1_2 ·BIPY is extended through weak CH_{Ph···}F and π_{BODIPY} ···F interactions that are perpendicular to the BODIPY plane. Additional CH_{Ph···} π interactions complete the supramolecular network.

The most striking aspect of the structure of $\mathbf{1}_2$ ·BIPY is the presence of only one HaB per 1. We were curious if this resulted from negative cooperativity in which binding on one side weakens binding on the other.⁴² This was probed computationally using pyridine to test the effects of HaB formation with $\mathbf{1}$ at one I atom on the V_{max} of the other. HaB formation caused a reduction in V_{max} of only ~15 kJ/mol from 86 kJ/mol. The stepwise binding energies were -25 kI/mol for the first pyridine and -24 kI/mol for the second. This suggests that minimal negative cooperativity occurs and simultaneous binding to both iodine atoms should not energetically prohibited. 1,2,4,5-Tetrafluoro-3,6diiodobenzene (C₆F₄I₂) is known to form two halogen bonds with pyridyl donors,43 and an equivalent analysis was performed on it. It was found that the V_{max} associated with the halogen bond donors were larger to begin with, 137 kJ/mol, and they experienced a larger decrease, 20 kJ/mol, upon forming a halogen bond. This indicates a greater degree of negative cooperativity with this smaller system. This is consistent with the stepwise binding energies, -38 kJ/mol for the first pyridine and -34 kJ/mol for the second.

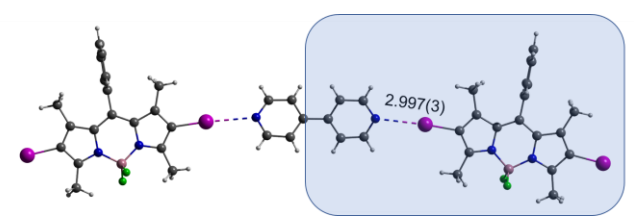


Figure 6. Supramolecular trimer of $\mathbf{1}_2$ -BIPY. Carbon, hydrogen, boron, nitrogen, fluorine, and iodine atoms are represented by gray, white, pink, blue, green, and purple, respectively. HaBs are depicted as hashed bonds. Blue shaded box depicts asymmetric unit. Distances in Å.

Solution-state binding

We sought to validate the computational method by measuring the solution phase binding of pyridyl HaB acceptors. Binding was monitored by through changes to the UV/vis spectrum upon titration with a HaB acceptor. In the case of pyridine, only a linear increase with the concentration of pyridine (following the Beer-Lambert Law) was observed preventing a meaningful analysis. Titration with 4-dimethylaminopyridine (DMAP) yielded a binding constant of 2470 M⁻¹ ($\Delta G = -19.4$ kJ/mol) when fit to a simple 1:1 binding model. A titration with BIPY gave a binding constant of 1070 M⁻¹ ($\Delta G = -17.3 \text{ kJ/mol}$) for 1:1 binding. These values are consistent with DMAP being a stronger HaB acceptor than BIPY. The value obtained for DMAP indicates that the HaB is weaker than the HB observed with a carboxylic acid44 but should outcompete the weak HB donors in 1.

DFT calculations suggested that both iodine atoms should be able to simultaneously participate in HaBs. A possible reason for the lack of infinite chains is that the size and shape mismatch between the two molecules prevents efficient crystal packing. This may account for the challenges with previous efforts to grow cocrystals of 1 with several nitrogen-based HaB acceptors, including monotopic, ditopic, and tetratopic molecules.⁴⁵

Size-matched cocrystal featuring 1 with BPA and anisotropic thermal expansion behavior

To test the size/shape match theory, 1 was crystallized with BPA, which is nearly identical in length to 1 and has a complementary shape that permits the two molecules to stack efficiently. The asymmetric unit contains two molecules each of 1 and BPA (Figure 7) denoted 1.BPA. In this case, the 1D chains do form by the anticipated I···N HaBs (avg. 3.051 Å at 190 K) coincident with the long axis of 1. These HaBs are slightly longer than those observed when BPA cocrystallizes with 1,4-diiodoperchlorobenzene (2.929(2) Å)⁴¹ and significantly longer than those involving electron-poor iodoethynylbenzene-based HaB donors or 1,4-diiodoperfluorobenzene (2.586(2) Å at 270 K).^{22,43,46} The molecules are further organized in the lattice through weak hydrogen bonding between the hydrogen atoms on the aromatic/pyridyl rings and the fluorine or iodine, coincident with the medium axis of the molecule. Sets of π - π interactions organize the molecules along their short axis, coincident with the b axis, to complete the structure. Notably, 1 and BPA stack with the acetylene group situated

between the 1 and 5 positions of $\mathbf{1}$, which appears to be important for the shape-matching of the two molecules. The IR spectrum lacks a peak associated with the $C \equiv C$ bond as expected for symmetrically substituted acetylenes (see Figure S14).

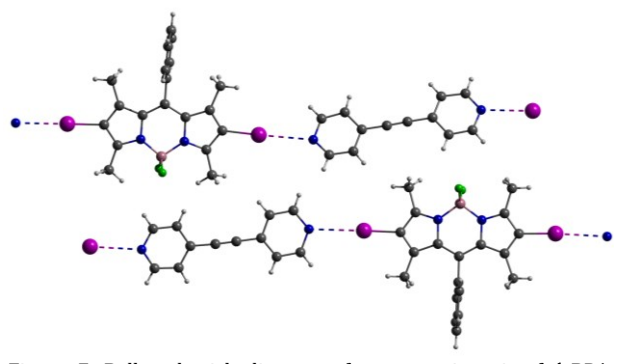


Figure 7. Ball and stick diagram of asymmetric unit of **1**·BPA. Carbon, hydrogen, boron, nitrogen, fluorine, and iodine atoms are represented by gray, white, pink, blue, green, and purple, respectively. HaBs are depicted as hashed bonds. Disorder in pyridine rings omitted for clarity.

The thermal expansion behavior of 1-BPA was investigated by calculating the principal axes of thermal expansion $(X_1,$ X₂, and X₃) and the thermal expansion coefficients using PASCal,⁴⁷ which accepts variable-temperature unit cell data as input. Three linear thermal expansion coefficients were obtained (α_{X1} , α_{X2} , α_{X3}), as well as a volumetric coefficient (α_v) (Table 1). The solid **1**·BPA undergoes the least thermal expansion along X₁, which coincides with the 1D HaB direction and the long axis of 1. A total of four unique I···N halogen bonds comprise the solid, and the halogen bonds increase in length as temperature is increased (Δ 0.02 to 0.06 Å). Slightly more expansion occurs along X2, which corresponds to the orthogonal, hydrogen-bonding axis of 1. A combination of C-H···F and C-H··· π interactions between and within stacked chains encompass the X2 direction. The weaker nature of these interactions leads to larger expansion along the direction. Colossal positive thermal expansion occurs along X₃, and the direction corresponds to the π - π stacking direction. The π - π interactions are the weakest of the three intermolecular forces used to assemble the solid. Thus, the orthogonal design strategy featuring three supramolecular interactions (HaB, HB, and π - π) successfully afforded a solid wherein different degrees of thermal expansion occurred along each bonding direction.

Table 1. Thermal expansion coefficients for the cocrystals over temperature range 190-290 K. The error is shown in parenthesis, and the approximate crystallographic plane is shown in brackets.

Cocrystal	α _{X1} (MK ⁻¹)	α _{X2} (MK ⁻¹)	α _{X3} (MK ⁻¹)	α _V (MK ⁻¹)
1·BPA	13 (1)	29 (1)	136 (2)	178 (1)
	[103]	[-100]	[0-10]	
1·BPE	10 (1)	21 (1)	148 (2)	179 (4)
	[-50-1]	[001]	[0-10]	
1·Azo (alpha)	12 (1)	34 (1)	148 (1)	194 (1)
	[-30-2]	[-506]	[0-10]	
1 ·Azo (beta)	-28 (12)	98 (3)	136 (5)	207 (5)
	[201]	[0-10]	[-105]	
1_2 ·Azo·BPE	17 (1)	26 (1)	150 (1)	194 (1)
	[-30-1]	[-104]	[0-10]	
1·Cl-Azo	15 (1)	52 (1)	124 (1)	192 (3)
	[-60-1]	[010]	[108]	

Cocrystals of 1 with motion-capable HaB acceptors

Previous studies have reported molecules containing groups that undergo molecular pedal motion^{48,49} can disrupt the interactions along the π stack and lead to changes in the thermomechanical properties.50-53 In an effort to exploit this, the current study was extended to include the ditopic HaB acceptors with similar topologies to BPA: BPE and Azo, and Cl-Azo (Figure 5). The cocrystals of these three bipyridines with 1 yield structures that are analogous to **1**·BPA. The structure of **1**·BPE is shown in Figure 8. The asymmetric unit contains two molecules of 1 and two molecules of BPE. Halogen bonds between the I and N_{BPE} atoms lead to infinite 1D chains that propagate approximately along with the [102] axis. Akin to the cocrystal with BPA, there are four unique HaBs in 1.BPE that range from 2.923-3.025 Å in length. These distances are approximately the same as those observed in the literature.⁵¹ The extended structure is isostructural with the BPA cocrystal, with one key difference: one of the two crystallographically unique molecules of BPE is disordered between 290-250 K and fully ordered from 230-190 K (Table 2). The change in site occupancies with change in temperature is indicative of dynamic motion within the solid, albeit the amount of motion is quite low. The IR spectrum confirmed the presence of the C=C with a stretch at 1594 cm⁻¹ (see Figure S15).

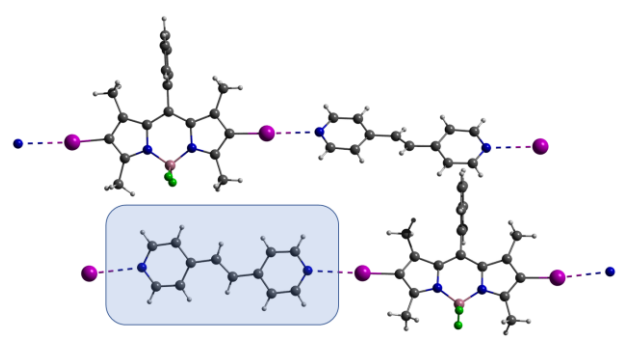


Figure 8. Ball and stick diagram of asymmetric unit of **1**·BPE. Carbon, hydrogen, boron, nitrogen, fluorine, and iodine atoms are represented by gray, white, pink, blue, green, and purple, respectively. HaBs are depicted as hashed bonds. Highlighted BPE displays disorder at elevated temperatures.

The thermal expansion behavior of $\mathbf{1}\cdot BPE$ is also anisotropic (Table 1). The least expansion occurs along the HaB direction, mild expansion occurs along the weak HB direction, and colossal expansion occurs along the $\pi-\pi$ stacking direction. The degree of expansion along X_1, X_2 , and X_3 for $\mathbf{1}\cdot BPE$ is similar to $\mathbf{1}\cdot BPA$. Notably, a small increase can be observed along X_3 where the thermal motion can disrupt the π stacking.

Table 2. Major site occupancies as a function of temperature for disordered HaB acceptor molecule within $1 \cdot BPE$, $\alpha \cdot 1 \cdot Azo$, and $1 \cdot Azo \cdot BPE$. In the ternary cocrystal, only the Azo component is disordered. The error is shown in parentheses.

Temperature (K)	1-BPE	α-1·Azo	1 ₂ ·Azo·BPE
290	0.92(1)	0.68(1)	0.75(1)
270	0.94(1)	0.71(1)	0.77(1)
250	0.94(1)	0.74(1)	0.78(1)
230	1.00	0.76(1)	0.79(1)
210	1.00	0.79(1)	0.80(1)
190	1.00	0.82(1)	0.84(1)

A cocrystal of **1** and Azo, shown in Figure 9, is also isostructural to the previous two cocrystals. Due to the observance of polymorphism (discussed below), this solid will be referred to as the alpha polymorph, α -**1**·Azo. The two molecules of **1** and two Azo molecules generate four distinct I···N HaBs with distances ranging from 2.962–3.090 Å. These are shorter than the HaBs observed in **1**·BPE. The FTIR analysis indicates a peak at 1586 cm⁻¹ verifying the presence of N=N stretching vibration as shown in Figure S16. One of the two crystallographically unique molecules of Azo is also disordered; however, the molecule is dynamically disordered over the entire temperature range (Table 2). The second crystallographically unique Azo molecule becomes disordered at 290 K (site occupancies 0.91:0.09).

 α -**1**·Azo also exhibits the same anisotropic thermal expansion behavior as **1**·BPA and **1**·BPE (Table 1). The expansion along X_2 and volumetrically is slightly larger than the previous two cocrystals, possibly due to occurrence of more significant molecular motion. Simultaneously,

increased expansion along X_3 is observed consistent with the pedal motion disrupting the π stacking.

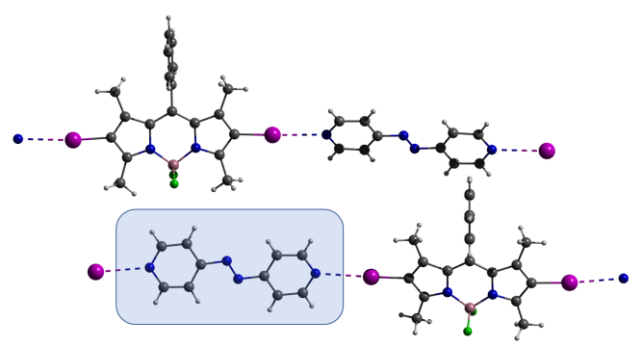


Figure 9. Ball and stick diagram of asymmetric unit of α -**1**·Azo. Carbon, hydrogen, boron, nitrogen, fluorine, and iodine atoms are represented by gray, white, pink, blue, green, and purple, respectively. HaBs are depicted as hashed bonds. Highlighted Azo displays dynamic disorder at all temperatures. Non-highlighted Azo only displays disorder at 290 K. Disorder omitted for clarity.

A second polymorph, β-1·Azo (Figure 10), was obtained from a toluene/ethanol solution of 1 and Azo (the components were dissolved in a 1:2 ratio). The two components assemble into the same type of supramolecular structure sustained by the same interactions; however, there is only one crystallographically unique molecule of 1 and Azo present in the asymmetric unit (instead of two, as in the other solids). The Azo molecule is also dynamically disordered over the entire temperature range (see experimental details in SI). Of all the compounds studied here, β -1·Azo was the only one to show negative thermal expansion along the X₁ axis. The negative expansion arises because the distance between molecules in the halogenbonded chains, which lie primarily along crystallographic a axis, decreases as the temperature increases. Large positive thermal expansion occurs along X2 and X₃. The X₂ expansion consists of C-H···F halogen bonds which resulted in a near-colossal TE, with a slight increase of 0.017 Å upon increasing the temperature. The dynamic motion along with larger changes in intermolecular interaction distances results in the significant expansion along X2 and X3.



Figure 10. Ball and stick diagram of asymmetric unit of β -1·Azo. Carbon, hydrogen, boron, nitrogen, fluorine, and iodine atoms are represented by gray, white, pink, blue, green, and purple, respectively. HaBs are depicted as hashed bonds, minor component of dynamically disordered Azo is faded.

The compound Cl-Azo (Figure 5) was isolated as an impurity in commercial Azo.⁵⁴ Cocrystallization of $\bf 1$ with Cl-Azo in a toluene/ethanol mixture afforded cocrystals that are isostructural with β - $\bf 1$ -Azo (Figure 11). The asymmetric unit

of 1.Cl-Azo consists of a molecule of 1 and a molecule of Cl-Azo. There are two unique halogen bonds with an I···N distance of 3.058 and 3.083 Å. 1·Cl-Azo showed moderate PTE along X_1 and X_2 , colossal PTE along X_3 , and colossal volumetric PTE. As with all other compounds in this study, the least expansion occurred along X₁, resulting from two unique I···N halogen bonds, which showed increases in interaction distances of 0.043 and 0.057 Å upon increasing the temperature. The X₂ expansion axis includes C-H···F halogen bonds, which showed an increase in distance of 0.026 Å upon increasing the temperature. The X_3 axis is dominated by C-H···Cl halogen bonding as well as π - π stacking, with both types of interactions showing moderate increases in distance upon increasing the temperature. The Cl-Azo molecule is statically disordered over two positions through a simple rotation. Evidence of pedal motion is not observed at any temperature. The lack of pedal motion could be due to the chloro substituent adjacent to the motion group, although pedal motion has been observed in stilbenes with ortho-substituted methyl groups.55

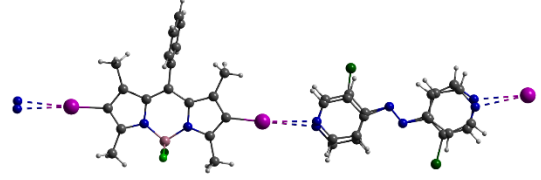


Figure 11. Ball and stick diagram of asymmetric unit of **1**·Cl-Azo. Carbon, hydrogen, boron, nitrogen, fluorine, and iodine atoms are represented by gray, white, pink, blue, green, and purple, respectively. HaBs are depicted as hashed bonds. Static disorder of the Cl-Azo unit is shown.

Ternary cocrystal based on molecular motion propensity

Given the isostructurality of $\mathbf{1}\cdot BPE$ and $\alpha \cdot \mathbf{1}\cdot Azo$ and the fact that two sets of crystallographically unique molecules are present in each asymmetric unit, we hypothesized that the system could offer a platform for synthesizing ternary cocrystals. In $\mathbf{1}\cdot BPE$, the olefin component is only slightly disordered at high temperature, whereas the azo

component in 1·Azo is disordered over the entire range. Thus, we hypothesized that differences in motion propensity would allow us to apply the *shape-size mimicry* strategy for synthesizing ternary cocrystals. This strategy was employed to form ternary cocrystals only a few other times, including examples by the groups of Desiraju in 1994, 2011 and 2014⁵⁶⁻⁵⁸ and Sustmann in 1999,⁵⁹ it relies on the substituting molecule to have a volumetric and interaction equivalence.^{57,60}

The ternary cocrystal $\mathbf{1}_2$ -Azo·BPE was prepared under the same conditions as the previous cocrystals, except a (2:1:1) stoichiometric mixture of $\mathbf{1}$, BPE, and Azo was used (Figure 12). Crystallographic analysis revealed that $\mathbf{1}_2$ -Azo·BPE was isostructural with $\mathbf{1}$ -BPE and α - $\mathbf{1}$ -Azo, confirming that the size-shape mimicry design strategy can be applied when the size/shape equivalency results from molecular motion in the solid state. The asymmetric unit of $\mathbf{1}_2$ -Azo·BPE consists of two molecules of $\mathbf{1}$ and one molecule each of Azo and BPE, where the two unique molecules of $\mathbf{1}$ HaB to either a unique molecule of BPE or a unique molecule of Azo. As such, this is different from examples that are considered non-

stoichiometric or solid solutions/organic alloys.⁶⁰ The I···N HaB distances between **1** and BPE were 2.944 and 3.018 Å, which are relatively shorter when compared to the I···N distances between **1** and Azo at 3.014 and 3.16 Å. FTIR analysis revealed two distinct peaks at 1594 and 1585 cm⁻¹ corresponding to C=C and N=N stretching vibrations, respectively, and confirming the presence of both Azo and BPE in the bulk phase (see Figure S17). Most importantly, the ternary cocrystal was achieved using differences in motion propensity. The Azo molecule sits in the disordered position and exhibits dynamic motion over the entire temperature range (Table 2). On the other hand, BPE lies in the ordered site and remains in one conformation at all temperatures.

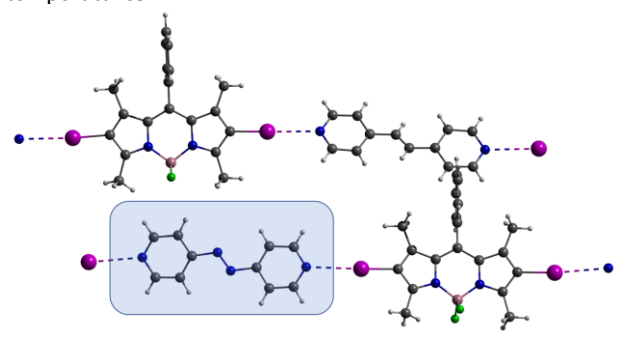


Figure 12. Ball and stick diagram of asymmetric unit of ternary cocrystal, **1**₂·Azo·BPE. Carbon, hydrogen, boron, nitrogen, fluorine, and iodine atoms are represented by gray, white, pink, blue, green, and purple, respectively. HaBs are depicted as hashed bonds. Highlighted Azo displays dynamic disorder at all temperatures, disorder omittedfor clarity.

 $\mathbf{1}_2$ ·Azo·BPE also exhibits anisotropic thermal expansion behavior (Table 1). The expansion along all three principal axes is similar in magnitude to the traditional two-component cocrystals, $\mathbf{1}$ ·BPE and α - $\mathbf{1}$ ·Azo.

3. CONCLUSION

An orthogonal self-assembly strategy was used to construct and control the anisotropy in the thermal expansion coefficients in organic binary and ternary solids of 1 and five different bipyridine coformers. Typically, there was an order of magnitude difference between the largest thermal expansion coefficient (which all exhibited colossal thermal expansion) and the smallest coefficient. Strategic incorporation of groups capable of molecular motion resulted in a 10% increase in the largest thermal expansion coefficient. Finally, a size-mimicry strategy based on propensity for solid-state molecular motion allowed for a rare example of a well-defined ternary cocrystal to be designed and studied. Orthogonal directing substitutents not only allow for control over solid-state self-assembly, but also afford control over material properties and achieving anisotropic behavior.

CONFLICTS OF INTEREST

There are no conflicts to declare.

AUTHOR CONTRIBUTIONS

BT prepared most crystals, JQ prepared **1** and ran solution state binding studies and DFT calculations, SM prepared **1**·BPA, GG performed thermal expansion analysis. BT, JQ and GG contributed to writing the manuscript. MCA and VW performed initial synthesis and preliminary studies. DKU performed crystallography. KMH and AFC conceived of study, analyzed data, wrote and edited manuscript.

ASSOCIATED CONTENT

Supporting Information

Synthesis and characterization, cocrystallizations, X-ray data, thermal expansion data, UV-Vis titrations, NMR analysis, DFT calculations. This material is available free of charge via the Internet at http://pubs.acs.org.

Accession Codes

CCDC 2306866-2306918 contain the supplementary crystallographic data for this paper. These data can be obtained free of charge via www.ccdc.cam.ac.uk/data_request/cif, or by emailing data_request@ccdc.cam.ac.uk, or by contacting The Cambridge Crystallographic Data Centre, 12 Union Road, Cambridge CB2 1EZ, UK; fax: +44 1223 336033.

AUTHOR INFORMATION

Corresponding Author

- * E-mail: anthony.f.cozzolino@ttu.edu; Fax: +1 806 742 1289; Tel: +1 806 834 1832
- * Email: kristin.hutchins@missouri.edu; Tel: +1 573 882 4598 Author Contributions

The manuscript was written through the contributions of all authors. All authors have approved the final version of the manuscript. †These authors contributed equally.

ACKNOWLEDGMENT

The present work was supported by Texas Tech University and the National Science Foundation (AFC research grant CHE-1847878, KMH research grant DMR-2045506, and NMR instrument grant CHE-1048553).

REFERENCES

- (1) Krishnan, R. S.; Srinivasan, R.; Devanarayanan, S. *Thermal Expansion of Crystals: International Series in the Science of the Solid State.* 1st ed.: Elsevier. 1979.
- (2) Roy, R.; Agrawal, D. K.; McKinstry, H. A. Very Low Thermal Expansion Coefficient Materials. *Annual Review of Materials Science* **1989**, 19 (1), 59–81. https://doi.org/10.1146/annurev.ms.19.080189.000423.
- (3) Engel, E. R.; Smith, V. J.; Bezuidenhout, C. X.; Barbour, L. J. Uniaxial Negative Thermal Expansion Facilitated by Weak Host–Guest Interactions. *Chem. Commun.* **2014**, *50* (32), 4238–4241. https://doi.org/10.1039/C4CC00849A.
- (4) Khalil, A.; Karothu, D. P.; Naumov, P. Direct Quantification of Rapid and Efficient Single-Stroke Actuation by a Martensitic Transition

- in a Thermosalient Crystal. *J. Am. Chem. Soc.* **2019**, *141* (8), 3371–3375. https://doi.org/10.1021/jacs.8b12752.
- (5) Panda, M. K.; Runčevski, T.; Chandra Sahoo, S.; Belik, A. A.; Nath, N. K.; Dinnebier, R. E.; Naumov, P. Colossal Positive and Negative Thermal Expansion and Thermosalient Effect in a Pentamorphic Organometallic Martensite. *Nat Commun* **2014**, *5* (1), 4811. https://doi.org/10.1038/ncomms5811.
- (6) Das, D.; Jacobs, T.; Barbour, L. J. Exceptionally Large Positive and Negative Anisotropic Thermal Expansion of an Organic Crystalline Material. *Nature Mater* **2010**, 9 (1), 36–39. https://doi.org/10.1038/nmat2583.
- (7) Lee, A. van der; Dumitrescu, D. G. Thermal Expansion Properties of Organic Crystals: A CSD Study. *Chem. Sci.* **2021**, *12* (24), 8537–8547. https://doi.org/10.1039/D1SC01076J.
- (8) Bond, A. D. A Survey of Thermal Expansion Coefficients for Organic Molecular Crystals in the Cambridge Structural Database. *Acta Cryst B* **2021**, *77* (3), 357–364. https://doi.org/10.1107/S2052520621003309.
- (9) Miller, W.; Smith, C. W.; Mackenzie, D. S.; Evans, K. E. Negative Thermal Expansion: A Review. *J Mater Sci* **2009**, *44* (20), 5441–5451. https://doi.org/10.1007/s10853-009-3692-4.
- (10) Takenaka, K. Progress of Research in Negative Thermal Expansion Materials: Paradigm Shift in the Control of Thermal Expansion. *Frontiers in Chemistry* **2018**, *6*.
- (11) Dharmarwardana, M.; Pakhira, S.; Welch, R. P.; Caicedo-Narvaez, C.; Luzuriaga, M. A.; Arimilli, B. S.; McCandless, G. T.; Fahimi, B.; Mendoza-Cortes, J. L.; Gassensmith, J. J. Rapidly Reversible Organic Crystalline Switch for Conversion of Heat into Mechanical Energy. *J. Am. Chem. Soc.* **2021**, *143* (15), 5951–5957. https://doi.org/10.1021/jacs.1c01549.
- (12) Kitaĭgorodskiĭ, A. I. *Molecular Crystals and Molecules*; Physical chemistry, a series of monographs; Academic Press: New York, 1973.
- (13) Rather, S. A.; Saraswatula, V. G.; Sharada, D.; Saha, B. K. Influence of Molecular Width on the Thermal Expansion in Solids. *New J. Chem.* **2019**, *43* (44), 17146–17150. https://doi.org/10.1039/C9NJ04888J.
- (14) Dwivedi, B.; Shrivastava, A.; Negi, L.; Das, D. Colossal Positive and Negative Axial Thermal Expansion Induced by Scissor-like Motion of a Two-Dimensional Hydrogen Bonded Network in an Organic Salt. *Crystal Growth & Design* **2019**, *19* (5), 2519–2524. https://doi.org/10.1021/acs.cgd.9b00145.
- (15) Liu, H.; Gutmann, M. J.; Stokes, H. T.; Campbell, B. J.; Evans, I. R.; Evans, J. S. O. Supercolossal Uniaxial Negative Thermal Expansion in Chloranilic Acid Pyrazine, CA-Pyz. *Chem. Mater.* **2019**, *31* (12), 4514–4523. https://doi.org/10.1021/acs.chemmater.9b01135.
- (16) Attfield, J. P. Mechanisms and Materials for NTE. *Frontiers in Chemistry* **2018**, *6*.
- (17) Burtch, N. C.; Baxter, S. J.; Heinen, J.; Bird, A.; Schneemann, A.; Dubbeldam, D.; Wilkinson, A. P. Negative Thermal Expansion Design Strategies in a Diverse Series of Metal–Organic Frameworks. *Advanced Functional Materials* **2019**, *29* (48), 1904669. https://doi.org/10.1002/adfm.201904669.
- (18) Teyssandier, J.; Mali, K. S.; De Feyter, S. Halogen Bonding in Two-Dimensional Crystal Engineering. *ChemistryOpen* **2020**, 9 (2), 225–241. https://doi.org/10.1002/open.201900337.
- (19) Cavallo, G.; Metrangolo, P.; Milani, R.; Pilati, T.; Priimagi, A.; Resnati, G.; Terraneo, G. The Halogen Bond. *Chem. Rev.* **2016**, *116* (4), 2478–2601. https://doi.org/10.1021/acs.chemrev.5b00484.
- (20) Corradi, E.; Meille, S. V.; Messina, M. T.; Metrangolo, P.; Resnati, G. Halogen Bonding versus Hydrogen Bonding in Driving Self-Assembly Processes. *Angewandte Chemie International Edition* **2000**, 39 (10), 1782–1786. https://doi.org/10.1002/(SICI)1521-3773(20000515)39:10<1782::AID-ANIE1782>3.0.CO;2-5.
- (21) González, L.; Gimeno, N.; Tejedor, R. M.; Polo, V.; Ros, M. B.; Uriel, S.; Serrano, J. L. Halogen-Bonding Complexes Based on Bis(Iodoethynyl)Benzene Units: A New Versatile Route to

- Supramolecular Materials. *Chem. Mater.* **2013**, *25* (22), 4503–4510. https://doi.org/10.1021/cm401849f.
- (22) Aakeröy, C. B.; Wijethunga, T. K.; Desper, J.; Đaković, M. Crystal Engineering with Iodoethynylnitrobenzenes: A Group of Highly Effective Halogen-Bond Donors. *Crystal Growth & Design* **2015**, *15* (8), 3853–3861. https://doi.org/10.1021/acs.cgd.5b00478.
- (23) Erdélyi, M. Halogen Bonding in Solution. *Chemical Society Reviews* **2012**, 41 (9), 3547–3557. https://doi.org/10.1039/C2CS15292D.
- (24) R. Treich, N.; D. Wimpenny, J.; A. Kieffer, I.; M. Heiden, Z. Synthesis and Characterization of Chiral and Achiral Diamines Containing One or Two BODIPY Molecules. *New Journal of Chemistry* **2017**, *41* (23), 14370–14378. https://doi.org/10.1039/C7NJ02670F.
- (25) Lee, Y.; Malamakal, R. M.; Chenoweth, D. M.; Anna, J. M. Halogen Bonding Facilitates Intersystem Crossing in Iodo-BODIPY Chromophores. *J. Phys. Chem. Lett.* **2020**, *11* (3), 877–884. https://doi.org/10.1021/acs.jpclett.9b03753.
- (26) Özcan, E.; Dedeoglu, B.; Chumakov, Y.; Gürek, A. G.; Zorlu, Y.; Çoşut, B.; Ayhan, M. M. Halogen-Bonded BODIPY Frameworks with Tunable Optical Features. *Chemistry A European Journal* **2021**, *27* (5), 1603–1608. https://doi.org/10.1002/chem.202003945.
- (27) Stafford, A.; Ahn, D.; Raulerson, E. K.; Chung, K.-Y.; Sun, K.; Cadena, D. M.; Forrister, E. M.; Yost, S. R.; Roberts, S. T.; Page, Z. A. Catalyst Halogenation Enables Rapid and Efficient Polymerizations with Visible to Far-Red Light. *J. Am. Chem. Soc.* **2020**, *142* (34), 14733–14742. https://doi.org/10.1021/jacs.0c07136.
- (28) Magagnano, G.; Gualandi, A.; Marchini, M.; Mengozzi, L.; Ceroni, P.; Cozzi, P. G. Photocatalytic ATRA Reaction Promoted by Iodo-Bodipy and Sodium Ascorbate. *Chem. Commun.* **2017**, *53* (10), 1591–1594. https://doi.org/10.1039/C6CC09387F.
- (29) Huang, L.; Zhao, J.; Guo, S.; Zhang, C.; Ma, J. Bodipy Derivatives as Organic Triplet Photosensitizers for Aerobic Photoorganocatalytic Oxidative Coupling of Amines and Photooxidation of Dihydroxylnaphthalenes. *J. Org. Chem.* **2013**, *78* (11), 5627–5637. https://doi.org/10.1021/jo400769u.
- (30) Li, W.; Li, L.; Xiao, H.; Qi, R.; Huang, Y.; Xie, Z.; Jing, X.; Zhang, H. Iodo-BODIPY: A Visible-Light-Driven, Highly Efficient and Photostable Metal-Free Organic Photocatalyst. *RSC Adv.* **2013**, *3* (32), 13417–13421. https://doi.org/10.1039/C3RA40932E.
- (31) Zhang, C.; Zhao, J.; Wu, S.; Wang, Z.; Wu, W.; Ma, J.; Guo, S.; Huang, L. Intramolecular RET Enhanced Visible Light-Absorbing Bodipy Organic Triplet Photosensitizers and Application in Photooxidation and Triplet-Triplet Annihilation Upconversion. *J. Am. Chem. Soc.* **2013**, 135 (28), 10566–10578. https://doi.org/10.1021/ja405170j.
- (32) Yogo, T.; Urano, Y.; Ishitsuka, Y.; Maniwa, F.; Nagano, T. Highly Efficient and Photostable Photosensitizer Based on BODIPY Chromophore. *J. Am. Chem. Soc.* **2005**, *127* (35), 12162–12163. https://doi.org/10.1021/ja0528533.
- (33) LeBlanc, L. E.; Gibbs, J. H.; Vicente, M. G. H.; Fronczek, F. R. CCDC 972982: Experimental Crystal Structure Determination. *Cambridge Crystallographic Data Centre*, 2013, 10.5517/cc11ngjp. https://doi.org/10.5517/cc11ngjp.
- (34) Gibbs, J. H.; Robins, L. T.; Zhou, Z.; Bobadova-Parvanova, P.; Cottam, M.; McCandless, G. T.; Fronczek, F. R.; Vicente, M. G. H. Spectroscopic, Computational Modeling and Cytotoxicity of a Series of Meso-Phenyl and Meso-Thienyl-BODIPYs. *Bioorganic & Medicinal Chemistry* **2013**, *21* (18), 5770–5781. https://doi.org/10.1016/j.bmc.2013.07.017.
- (35) Sabatini, R. P.; Lindley, B.; McCormick, T. M.; Lazarides, T.; Brennessel, W. W.; McCamant, D. W.; Eisenberg, R. Efficient Bimolecular Mechanism of Photochemical Hydrogen Production Using Halogenated Boron-Dipyrromethene (Bodipy) Dyes and a Bis(Dimethylglyoxime) Cobalt(III) Complex. *J. Phys. Chem. B* **2016**, *120* (3), 527–534. https://doi.org/10.1021/acs.jpcb.5b11035.
- (36) Swaminathan, S.; Fowley, C.; Thapaliya, E. R.; McCaughan, B.; Tang, S.; Fraix, A.; Captain, B.; Sortino, S.; Callan, J. F.; Raymo, F. M.

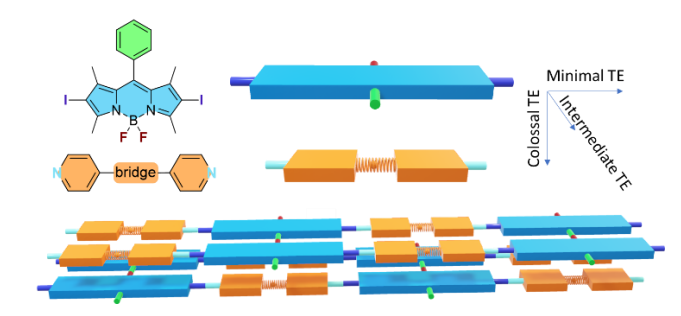
- Supramolecular Nanoreactors for Intracellular Singlet-Oxygen Sensitization. *Nanoscale* **2015**, 7 (33), 14071–14079. https://doi.org/10.1039/C5NR02672E.
- (37) Bond, A. D. What Is a Co-Crystal? *CrystEngComm* **2007**, *9* (9), 833–834. https://doi.org/10.1039/B708112J.
- (38) Etter, M. C. Encoding and Decoding Hydrogen-Bond Patterns of Organic Compounds. *Acc. Chem. Res.* **1990**, *23* (4), 120–126. https://doi.org/10.1021/ar00172a005.
- (39) Desiraju, G. R. Supramolecular Synthons in Crystal Engineering—A New Organic Synthesis. *Angewandte Chemie (International ed. in English)* **1995**, 34 (21), 2311–2327. https://doi.org/10.1002/anie.199523111.
- (40) Wu, W.; Guo, H.; Wu, W.; Ji, S.; Zhao, J. Organic Triplet Sensitizer Library Derived from a Single Chromophore (BODIPY) with Long-Lived Triplet Excited State for Triplet-Triplet Annihilation Based Upconversion. *J. Org. Chem.* **2011**, *76* (17), 7056–7064. https://doi.org/10.1021/jo200990y.
- (41) Bosch, E.; Kruse, S. J.; Krueger, H. R.; Groeneman, R. H. Role of π - π Stacking and Halogen Bonding by 1,4-Diiodoperchlorobenzene To Organize the Solid State To Achieve a [2 + 2] Cycloaddition Reaction. *Crystal Growth & Design* **2019**, *19* (6), 3092–3096. https://doi.org/10.1021/acs.cgd.9b00275.
- (42) Moaven, S.; Andrews, M. C.; Polaske, T. J.; Karl, B. M.; Unruh, D. K.; Bosch, E.; Bowling, N. P.; Cozzolino, A. F. Triple-Pnictogen Bonding as a Tool for Supramolecular Assembly. *Inorg. Chem.* **2019**, *58* (23), 16227–16235. https://doi.org/10.1021/acs.inorgchem.9b02761.
- (43) Hutchins, K. M.; Unruh, D. K.; Carpenter, D. D.; Groeneman, R. H. Thermal Expansion along One-Dimensional Chains and Two-Dimensional Sheets within Co-Crystals Based on Halogen or Hydrogen Bonds. *CrystEngComm* **2018**, *20* (45), 7232–7235. https://doi.org/10.1039/C8CE01090K.
- (44) Loya, J. D.; Qiu, J.; Unruh, D. K.; Cozzolino, A. F.; Hutchins, K. M. Co-Crystallization of the Anti-Cholesterol Drug Bezafibrate: Molecular Recognition of a Pharmaceutical Contaminant in the Solid State and Solution via Hydrogen Bonding. *Crystal Growth & Design* **2018**, *18* (9), 4838–4843. https://doi.org/10.1021/acs.cgd.8b00812.
- (45) Gümüşgöz Çelik, G.; Dedeoglu, B.; Gürek, A. G.; Zorlu, Y.; Ayhan, M. M. Enhancing Supramolecular Assembly in BODIPY Derivatives: Harnessing Halogen Bonding for Cocrystal Design. *Crystal Growth & Design* **2023**, *23* (10), 7285–7294. https://doi.org/10.1021/acs.cgd.3c00663.
- (46) Nguyen, S. T.; Rheingold, A. L.; Tschumper, G. S.; Watkins, D. L. Elucidating the Effects of Fluoro and Nitro Substituents on Halogen Bond Driven Assemblies of Pyridyl-Capped π -Conjugated Molecules. *Crystal Growth & Design* **2016**, *16* (11), 6648–6653. https://doi.org/10.1021/acs.cgd.6b01321.
- (47) Cliffe, M. J.; Goodwin, A. L. *PASCal*: A Principal Axis Strain Calculator for Thermal Expansion and Compressibility Determination. *J Appl Crystallogr* **2012**, *45* (6), 1321–1329. https://doi.org/10.1107/S0021889812043026.
- (48) Harada, J.; Ogawa, K. Pedal Motion in Crystals. *Chem. Soc. Rev.* **2009**, *38* (8), 2244–2252. https://doi.org/10.1039/B813850H.
- (49) Harada, J.; Ogawa, K. Invisible but Common Motion in Organic Crystals: A Pedal Motion in Stilbenes and Azobenzenes. *J. Am. Chem. Soc.* **2001**, *123* (44), 10884–10888. https://doi.org/10.1021/ja011197d.
- (50) Hutchins, K. M.; Unruh, D. K.; Verdu, F. A.; Groeneman, R. H. Molecular Pedal Motion Influences Thermal Expansion Properties within Isostructural Hydrogen-Bonded Co-Crystals. *Crystal Growth & Design* **2018**, *18* (2), 566–570. https://doi.org/10.1021/acs.cgd.7b01386.
- (51) Juneja, N.; Unruh, D. K.; Bosch, E.; Groeneman, R. H.; Hutchins, K. M. Effects of Dynamic Pedal Motion and Static Disorder on Thermal Expansion within Halogen-Bonded Co-Crystals. *New J. Chem.* **2019**, *43* (47), 18433–18436. https://doi.org/10.1039/C9NJ04833B.
- (52) Ding, X.; Unruh, D. K.; Groeneman, R. H.; Hutchins, K. M. Controlling Thermal Expansion within Mixed Cocrystals by Tuning

- Molecular Motion Capability. *Chem. Sci.* **2020**, *11* (29), 7701–7707. https://doi.org/10.1039/D0SC02795B.
- (53) George, G. C.; Unruh, D. K.; Groeneman, R. H.; Hutchins, K. M. Molecular Motion and Ligand Stacking Influence Thermal Expansion Behavior and Argentophilic Forces in Silver Coordination Complexes. *Crystal Growth & Design* **2022**, *22* (7), 4538–4545. https://doi.org/10.1021/acs.cgd.2c00446.
- (54) Mazzeo, P. P.; Carraro, C.; Arns, A.; Pelagatti, P.; Bacchi, A. Diversity through Similarity: A World of Polymorphs, Solid Solutions, and Cocrystals in a Vial of 4,4'-Diazopyridine. *Crystal Growth & Design* **2020**, *20* (2), 636–644. https://doi.org/10.1021/acs.cgd.9b01052.
- (55) Harada, J.; Ogawa, K. What Molecules Are Likely or Unlikely To Undergo Pedal Motions in Crystals? *Crystal Growth & Design* **2014**, *14* (10), 5182–5188. https://doi.org/10.1021/cg500962y.
- (56) Reddy, D. S.; Craig, D. C.; Desiraju, G. R. Organic Alloys: Diamondoid Networks in Crystalline Complexes of 1,3,5,7-Tetrabromoadamantane, Hexamethylenetetramine and Carbon Tetrabromide. *J. Chem. Soc., Chem. Commun.* **1994**, No. 12, 1457–1458. https://doi.org/10.1039/C39940001457.
- (57) Tothadi, S.; Mukherjee, A.; Desiraju, G. R. Shape and Size Mimicry in the Design of Ternary Molecular Solids: Towards a Robust Strategy for Crystal Engineering. *Chem. Commun.* **2011**, *47* (44), 12080–12082. https://doi.org/10.1039/C1CC14567C.
- (58) Chakraborty, S.; Rajput, L.; Desiraju, G. R. Designing Ternary Co-Crystals with Stacking Interactions and Weak Hydrogen Bonds. 4,4′-Bis-Hydroxyazobenzene. *Crystal Growth & Design* **2014**, *14* (5), 2571–2577. https://doi.org/10.1021/cg500263g.
- (59) Smolka, T.; Boese, R.; Sustmann, R. Design of a Three Component Crystal Based on the Cocrystal of Phenazine and 2,2′-Dihydroxybiphenyl. *Structural Chemistry* **1999**, *10* (6), 429–431. https://doi.org/10.1023/A:1022427122156.
- (60) Mir, N. A.; Dubey, R.; Desiraju, G. R. Strategy and Methodology in the Synthesis of Multicomponent Molecular Solids: The Quest for Higher Cocrystals. *Acc. Chem. Res.* **2019**, *52* (8), 2210–2220. https://doi.org/10.1021/acs.accounts.9b00211.

For Table of Contents Use Only

Combining molecular motion with a 2,6-diiodo BODIPY to engineer highly anisotropic thermomechanical properties in organic binary and ternary molecular materials

Babak Tahmouresilerd, Jinchun Qiu, Gary C. George III, Vivian Woh, Miranda C. Andrews, Shiva Moaven, Daniel K. Unruh, Kristin M. Hutchins, and Anthony F. Cozzolino



Synopsis:

A strategy for designing organic solid-state materials with anisotropic thermomechanical behaviors is described. A BODPIY core strategically decorated with orthogonal hydrogen- and halogen-bond donor groups is cocrystallized with a series of halogen-bond acceptors that are size-matched with the BODIPY. A rare ternary cocrystal isostructural to the two binary solids was achieved by employing shape-size mimicry and propensity for molecular motion.